Combustion and Flame 177 (2017) 37–48

Contents lists available at ScienceDirect

Combustion and Flame

journal homepage: www.elsevier.com/locate/combustflame

Dissociative influence of H_2O vapour/spray on lean blowoff and NO_x reduction for heavily carbonaceous syngas swirling flames

D.G. Pugh*, P.J. Bowen, R. Marsh, A.P. Crayford, J. Runyon, S. Morris, A. Valera-Medina, A. Giles

Cardiff School of Engineering, Cardiff University, Wales, UK

ARTICLE INFO

Article history:
Received 7 June 2016
Revised 21 July 2016
Accepted 9 November 2016

Keywords:
Turbulent lean premixed flames
Humidified syngas combustion
Chemical kinetics
OH-PLIF
Emissions
Converter gas

ABSTRACT

Recent studies have described and evidenced the enhancement of fundamental combustion parameters such as laminar flame speed due to the catalytic influence of H_2O with heavily carbonaceous syngas mixtures. In this study, the potential benefits of these subtle changes in water loading and hence reaction pathways are explored in terms of delayed lean blowoff, and primary emission reduction in a premixed turbulent swirling flame (Ø = 0.6–0.8), scaled for practical relevance. Chemical kinetic models initially confirm that H_2O has a substantial impact on the employed fuel behaviour; increasing flame speed by up to 60% across an experimental range representative of fluctuation in atmospheric humidity (~1.8 mol%). OH* chemiluminescence and OH planar laser induced fluorescence (PLIF) were employed to analyse the changes in heat release structure resulting from the experimental addition of H_2O vapour to the combustor. Equivalent concentrations of liquid H_2O were introduced into the central recirculation zone of the premixed flame as an atomised spray, to investigate the influence of phase changes on the catalytic effect. Near the lean stability limit, H_2O addition compresses heat release to shorten the elongated flame structure. Whereas with a stable and well-defined flame structure, the addition triggers a change in axial heat release location, causing the flame front to retract upstream toward the burner outlet. Higher quantities of two-phase flow were combined to explore the possibility of employing the spray as a stabilising mechanism, effectively dampening the observed influence of humidity. The chemical enhancement induced by the controlled supply was shown to reduce the lean blowoff stability limit, enabling an increase in additional air flow of almost 10%. However, the catalytic effect of H_2O diminishes with excessive supply and thermal quenching prevails. There is a compound benefit of NO_x reduction from the use of H_2O as a flame stabiliser with the practically-relevant syngas: First NO_x production decreases due to thermal effect of H_2O addition, with potential for further reduction from the change in lean stability limit; leanest experimental concentrations reduced by up to a factor of four with two-phase flow at the highest rates of supply. Hence, the catalytic effect of H_2O on reaction pathways and reaction rate predicted and observed in the laminar environment, is shown to translate into practical benefits in the challenging environment of turbulent, swirl-stabilised flames.

1. Introduction

Heavily carbonaceous converter gas typically comprises 50–80% CO, 10–18% CO_2, 1–3% H_2 in a balance of N_2 (mol%) [1,2]. The influence of water content on combustion performance for this increasingly utilised fuel is highly relevant [2–9], as it provides a potential dissociative catalytic influence on CO oxidation [3,4] across a limited water loading range. Direct formation of CO_2 from CO is slow due to high activation energy, and the presence of hydrogen facilitates chain branching OH formation, changing the dominant path for oxidation [4]. This contrasts with a lowering of adiabatic flame temperature. Water addition therefore induces a competition between chemical and thermal effects over a limited range. This provides a non-monotonic influence on premixed flame propagation, increasing laminar flame speed and reaction rate at lower concentrations, before eventually diluting and slowing the reaction as loading increases. Recent studies undertaken with a converter gas mixture demonstrated the potential for large increases in laminar flame speed – up to 70% – with the

* Corresponding author.
E-mail address: pughdg@Cardiff.ac.uk (D.G. Pugh).

http://dx.doi.org/10.1016/j.combustflame.2016.11.010

addition of water vapour, as concentrations varied by amounts representative of change in atmospheric humidity [4]. This level of fluctuation would be expected to provide a significant impact on the behaviour of converter gas in practical application.

1.1. Aim of this work

With previous emphasis on the fundamental laminar premixed behaviour of the applied fuel mixture [3,4], the aim of the current investigation is to appraise to what extent these potentially positive features extend to the practical environment of turbulent, premixed swirling flames supplied with a similar representative fuel composition. Clearly whilst the laminar flame characteristics provide an indication of fuel behaviour in turbulent swirling flames, these also introduce further complexity, for example the influence on flow dynamics and flame stretch [10,11]. Nevertheless, in a qualitative sense, the laminar studies indicate that practical benefits such as extended flame blowoff limit, and improved NO_x emission performance for swirl burners are likely [12–15]. Variation in these performance characteristics are quantified within this study.

Water vapour concentration was varied initially across a range equivalent to change in atmospheric humidity, as a fraction of the total reactant flow (up to ~1.8 mol% of total reactant composition). This allowed potential fluctuations in flame behaviour to be studied, within a range of practical relevance. This change in behaviour was analysed using advanced optical diagnostic techniques; namely OH* chemiluminescence, and OH planar laser induced fluorescence (PLIF) [16–18] enabling evaluation of any variation in local heat release, in addition to the formation of intermediate OH previously shown to accelerate the reaction [3,4]. The net thermal power of the flame from the generic swirl burner employed was maintained at 100 kW throughout.

The experimental setup was designed so water could be introduced into the system either as a vapour or an atomised liquid spray – delivered into the central recirculation zone of the swirling flow – or both. Potential differences in the catalytic behaviour resulting from the H_2O phase change could then be studied for its direct influence on flame stability. Finally, two-phase parametric studies were conducted to examine the effectiveness of employing a central recirculation spray to reduce the vapour-induced enhancements in dry flame behaviour. In addition to flame stability, the production of gaseous emissions was also quantified, with attention given to NO_x formation.

2. Experimental facilities

2.1. Burner assembly

Experiments were undertaken using a premixed generic swirl burner, housed within a high pressure optical chamber (HPOC) at Cardiff University's Gas Turbine Research Centre (GTRC). The burner and casing assembly are shown as a multi-component schematic in Fig. 1.

The burner assembly has been modified from previous work [16], with the addition of a centreline liquid injection lance (Fig. 1(a)); water is supplied from a pressurised 20 L accumulator in the range of 0.7–2.2 MPa, with delivery measured using an inline Coriolis mass-flow meter (Emerson CMF010M ± 0.1%). Reactants enter the burner inlet plenum (Fig. 1(b)) via fixed piping or flexible metallic hose, with mass flows again quantified using Coriolis meters (Emerson CMF025M ± 0.35%). When steam is required, liquid flow is regulated using a Bronkhorst mini CORI-FLOW controller (± 0.2%), before changing phase in a 25 m heated supply line. The burner assembly is housed within a pressure casing (Fig. 1(c)) rated to 1.6 MPa at 900 K. After entering the plenum, reactants travel through the premix chamber (Fig. 1(d)) to a single radial-tangential swirler (Fig. 1(e)) and out the burner exit nozzle (20 mm radius). The outlet has a geometric swirl number (ratio of tangential to axial momentum) equivalent to $S_g = 1.04$ [19,20]. A Delevan 0.4 hollow cone (W) 60° spray nozzle was installed on the liquid injection lance to provide atomised water droplets, positioned to spray into the CRZ of the outlet flow field, and released in the same plane as the 40 mm diameter burner outlet (Fig. 1(f) – spray is characterised further in Section 3). Optical access is afforded via diametrically opposed quartz viewing windows (Fig. 1(g)), facilitating the chemiluminescent and PLIF diagnostic techniques. The burner is operated with cylindrical quartz exhaust confinement tube, with an expansion ratio of 3.5 from the burner nozzle exit (Fig. 1(h)). The exhaust is then sampled downstream of the confinement in a temperature conditioned probe, detailed further in Section 2.4. Several k and n-type thermocouples (± 2.2 K) were installed to monitor key rig temperatures, influential to the experimental output. The first thermocouple is housed in the inlet plenum (T1) feeding into the premix swirl chamber, and monitors the temperature of reactants entering the system. A second thermocouple mounted flush with the burner face (T2) provides a reading for the recirculated and radiated heat from combustion. Finally, a third measurement is made at the burner exit (T3) giving exhaust temperature at the quartz tube outlet.

2.2. OH* chemiluminescence measurements

The chemiluminescence of an excited hydroxyl (OH) intermediate radical (wavelength of ~310 nm) can be used to provide a non-intrusive qualitative indication of localised heat release, and a generalised marker of flame front location [16–18]. For the purposes of this work, the relatively weak OH* signal was captured using a Dantec Dynamics Hi Sense Mk II CCD camera with a 1.3 megapixel resolution, coupled to a Hamamatsu C9546-03 L image intensifier. A specialty 78 mm focal length UV lens (F-stop = f/3.8) was installed on the aforementioned image intensifier, together with a narrow band pass filter (300–330 nm). The camera is placed at a 90° angle to the flow such that the flame can be viewed through the top quartz window of the HPOC (Fig. 1). The image plane is centred on the burner exit, with respective view fields of ~100 mm and ~75 mm in the radial and axial directions, corresponding to a resolution of ~13.6 pix/mm. For each experiment, 200 images were captured at a rate of 10 Hz with the system timing controlled using commercial software and a gate pulse generator set at 400 µs, triggered by the camera aperture signal. To ensure consistency between OH* chemiluminescence measurements, the gain of the image intensifier was held constant for all experiments. The intensities measured for the 200 image dataset were averaged, with a condition-normalised false colourmap (correlated to relative pixel signal intensity) then applied, to help provide an indication of the flame front location and localised heat release.

The axial flow field generated by the employed swirl configuration has been previously evaluated using particle image velocimetry [21], with a planar representation at the nozzle centreline shown in Fig. 2(a). The flame structure is typical for a premixed swirler of this design [22], with outward forward flow (orange in Fig. 2(a)) generating a conical flame around a shear layer of zero axial velocity, and central recirculation zone (CRZ – blue in Fig. 2(a)). The observed OH* chemiluminescence is taken line-of-sight, meaning the captured image includes light emitted both in front, and behind the focal plane of the imaging system. Thus, in the case of the swirl-stabilised flames evaluated in this work, the resulting images show intensity from the three-dimensional, conical shape of the flame (Fig. 2(b)). A modified open access Abel inversion algorithm [23] was used to transform the 3-D images captured into 2-D planar representations of the OH* chemiluminescence intensity distribution, with the underlying

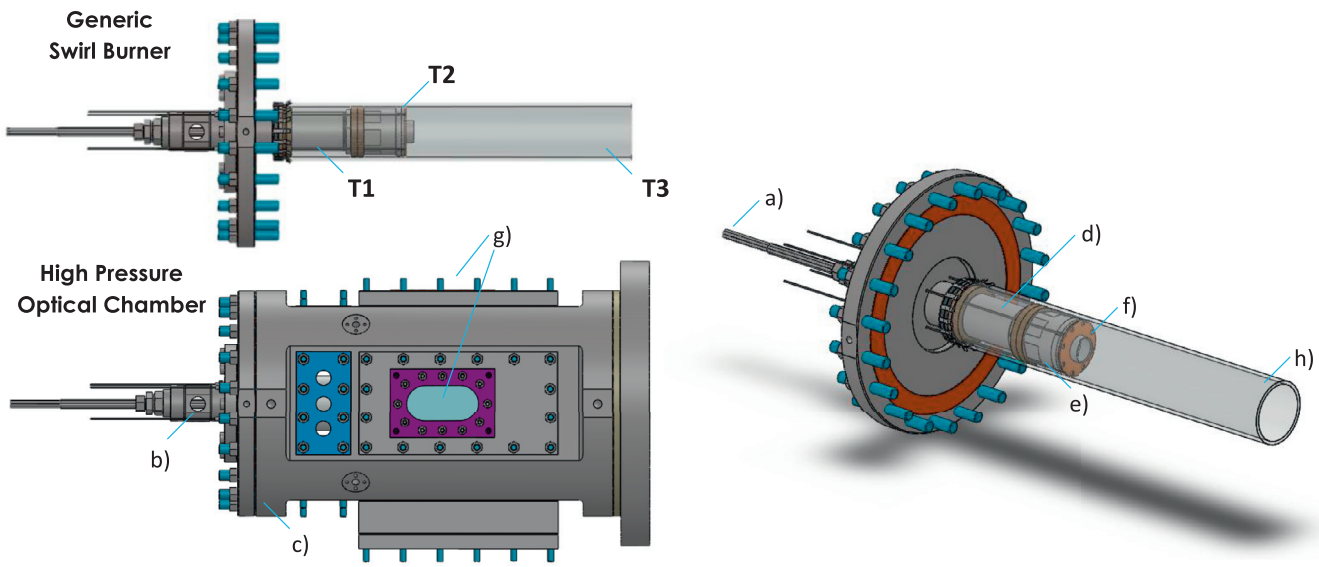

Fig. 1. Multi-component schematic of the burner assembly and optical casing (components are described in the text).

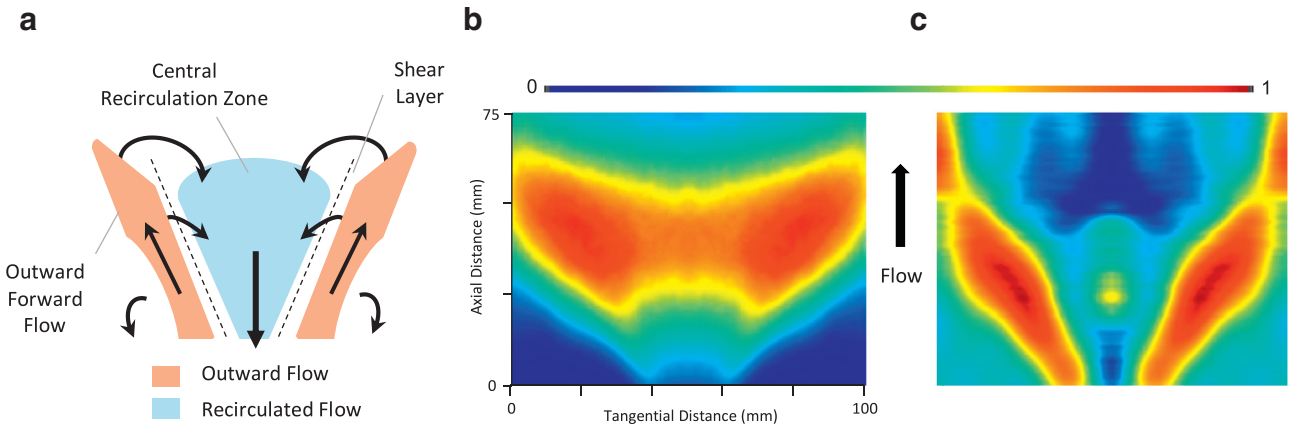

Fig. 2. Simplified planar representation of the axial flow field at the nozzle centreline (a), with a comparison between full OH* flame chemiluminescence (b), and the equivalent Abel transformed image (c).

assumption that the swirl-stabilised flame is axisymmetric about its centreline (Fig. 2(c)) [22–25]. Both raw chemiluminescence, and Abel deconvoluted images are presented for the undertaken experiments, with an example of the symmetric flame shown for comparison in Fig. 2 (figure is oriented so flow is from the bottom up, with intensities normalised to the image maximum). Detailed information regarding the chemiluminescence image capture system and processing technique can be found in [25].

2.3. Planar laser induced fluorescence (PLIF) measurements

In addition to OH* chemiluminescence, qualitative planar laser induced fluorescence (PLIF) measurements were also obtained for each experimental condition. The PLIF system comprises a Quantel TDL-90 dye laser pumped by the 532 nm output beam of a frequency-doubled Spectra Physics GCR 170-10 Nd:YAG laser operating at 10 Hz. The output beam of the TDL-90 was tuned to 283 nm to excite the (1,0) band of the OH radical, while fluorescence was captured at 315 nm through the use of the same intensified CCD camera system as listed for the OH* chemiluminescence measurements above. The output beam from the dye laser was then directed through a set of telescopic sheet-forming optics to provide a laser sheet 25 mm in width. This entered the test rig through a side window of the HPOC while the CCD camera was focussed on the burner nozzle centreline, through the top window of the HPOC, perpendicular to both the laser sheet and fluid flow. This system produces pulse energies of roughly 16 mJ/pulse at 283 nm, which is critical for the test rig setup given the size and shape of the HPOC windows, and the quartz confinement tube. Given the short lifetime of the OH radical fluorescence signal and influence of quenching effects, the gate timing of the image intensifier was set to 1.5 μs, triggered by the Q-switch of the Nd:YAG laser to ensure that signal capture was appropriately timed with the laser excitation light pulse. The image intensifier gain was held constant at all test conditions to ensure comparability, while reducing signal to noise ratio as much as possible. For each test condition, 500 images were taken at a rate of 10 Hz, with the same approximate view fields and pixel resolution as the OH* chemiluminescence images. The obtained image intensities were again temporally averaged, and corrected for background reflected light for presentation. The uncertainties in obtaining quantitative PLIF measurements are significant, with correction required for changes in collisional quenching and temperature [26] for each condition of the employed experimental specification. Qualitative

results were therefore analysed for relative change in normalised OH concentration profiles as markers for flame location and stability, similar to other equivalent works [22,27].

2.4. Exhaust emissions measurements

The exhaust stream was sampled using an equal area probe (9 holes) water conditioned to 433 K, and located approximately 10 diameters downstream of the quartz combustor exit, in accordance with ISO 11042 [28]. The probe, sample line, filter and distribution manifolds were maintained at 433 K, with a heated pump used to deliver products to the analysis suite. Total NO_x concentrations were quantified using a heated vacuum chemiluminescence analyser (Signal Instruments 4000VM), calibrated in the range 0–39 ppmV. Concentrations were measured hot and wet to avoid any water absorption losses, with data normalised to equivalent dry conditions prior to presentation. A flame ionisation detector (Signal Instruments 3000HM) was also employed to measure unburned hydrocarbons at C_3H_8 equivalent concentrations in the heated gas stream. Additional sample was directed to a chiller, used to reduce the molar water concentration below 1% before downstream CO and O_2 measurements were made using a combination of nondispersive infrared and paramagnetic analysers (Signal instruments 9000MGA). These were calibrated in the respective ranges of 0–904 ppmV, and 22.52%vol.

3. Specification of experimental conditions

Fuel fractions were taken from previous work [2,4], and comprised a molar composition of 65% CO, 1% H_2 and a combined diluent fraction of 34% N_2. All measurements were made at atmospheric pressure, and 100 kW net thermal power (a constant fuel mass flow rate of 14.9 g s^{-1}) for three initial equivalence ratios (Ø) in the range 0.6–0.8 (air flows of 30.4–40.2 g s^{-1}). This was specified with consideration given to performance of the liquid spray nozzle: A maximum flow of 0.52 g s^{-1} could be achieved from the accumulator at 2.2 MPa supply pressure, and the experiment was designed so that water concentrations were varied to levels representative of change in atmospheric humidity. Allowing for the equivalence ratio specification, 100 kW thermal power meant volumetric flow increases of 1.5–1.8% with water addition. With respect to the overall reactant composition; this was equivalent to a relative humidity of ~50% at 298 K, or fully saturated at 288 K, and therefore offered conditions in a range representative of practical application. Fully vaporised, the addition of water also resulted in a most significant (realised at Ø = 0.8, when relative fraction is highest as airflow is reduced) density reduction of 0.65%, and isobaric heat capacity increase of 0.27% for the overall reactant mixture. The influence of water addition on flow dynamics was therefore minimal compared to the change in chemical timescales.

The design characteristics of the nozzle also provided a limitation on the lowest possible flow sprayed into the flame, corresponding to 0.32 g s^{-1} at 0.7 MPa. Commissioning trials were performed, and supply pressures under this value resulted in poor atomisation and a limited spray cone definition. Therefore an intermediate test point equivalent to 0.42 g s^{-1} was finally specified for the liquid spray case. Water droplet SMDs were expected to vary between approximately 75 and 90 µm [29] for the given nozzle and pressure range specification, with ~17% smaller droplets produced at the highest pressure. However it should be noted that data were obtained without a flame, with performance at hotter conditions unquantified. For the fully vaporised experiments, the same flow rates were defined for comparison, with the exception of the 0.42 g s^{-1} case. Instead the flow was reduced by the equivalent full scale margin to 0.12 g s^{-1}, to provide an intermediate measurement with a lower flow rate. Finally both methods of H_2O addition were combined to give a maximum of 0.94 g s^{-1}, and analyse the spray influence on an already humidified premixed reactant flow.

Fuel was supplied from gravimetrically blended cylinder packs, produced in the same batch with a 1% full-scale uncertainty of each mixture component. The cylinders were constructed from aluminium to minimise the potential for iron pentacarbonyl formation from the pressurised storage of carbon monoxide. Combustion air was supplied from an Atlas Copco GA 45 VSD compressor. Prior to entering the distribution pipework, the compressed air was dried using a Beko Drypoint DPRA960. The dew point at the inlet plenum was measured using a Michell Instruments S3000 hygrometer, returning values in the range of −19 to −17 °C equivalent to ~1300 to ~1600 ppmV H_2O, which gave the baseline 'dry' condition. In addition, combustion air was analysed using the flame ionisation detector for hydrocarbon contamination as part of the experimental setup procedure. Concentrations were minimal, and typically measured in the range 0–1 ppmV C_3H_8 equivalent. The entire experimental system was warmed for up to one hour to reduce some of the effects of local heat loss, evaluated by monitoring the exhaust temperature, T3 in Fig. 1. Nominally equivalent measurements were taken at various stages throughout the programme with minimal temperature variation noted ~2%. In addition, the inlet plenum temperature (T1, Fig. 1) was monitored, and typically ~300 ± 3 K, with an increase of up to ~20 K resulting from the introduction of steam to the premixed reactants.

The lean stability limit (lean blowoff, or LBO point) was also evaluated for each experimental condition. This was defined by the equivalence ratio that resulted in detachment from the outlet nozzle to give a lifted flame, stabilising downstream in the quartz confinement tube with increased air flow. This was obtained by incrementally increasing air flow via a digitally controlled needle valve giving steps of ~0.2 g s^{-1}, and visually monitoring the flame response.

4. Results and discussion

4.1. Modelling reaction kinetics

Chemical kinetic models were obtained using the PREMIX [30] program in the CHEMKIN-PRO [31] laminar flame speed calculator to provide 1-D simulations of intermediate reaction chemistry, and help understand and analyse the expected premixed flame response. The calculation employed the modified Davis et al. [32] reaction mechanism (MDM) developed recently [4], optimised for use with humidified syngas compositions, and comprises 14 chemical species and 38 reactions. Unlike the previous work, this study focussed on lean conditions to explore lean blowoff in particular, and hence combustion was modelled for the three specified equivalence ratios (Ø = 0.6, 0.7, and 0.8). Solutions are based on an adaptive grid of 1000 points, with mixture-averaged transport properties and trace series approximation. For converter gas, water has been shown to provide two competing influences on premixed flame propagation; first it acts as a diluent and the reaction is slowed by a reduction in adiabatic flame temperature [4]. The second effect results from changes in flame thermochemistry, and an increase in overall reaction rate due to the dissociative production of chain carrying species (such as OH), and enhanced heat release rate. The catalysing effect of these radicals on CO consumption processes have been shown to reduce the slow reaction (with high activation energy): $CO+O_2 \rightarrow CO_2+O$ [2,4]. Figures 3 and 4 show the respective changes in predicted adiabatic flame temperature and maximum heat release rate (HRR) for the employed fuel composition. Note that for consistency results have been plotted against overall mixture H_2O fraction, with the

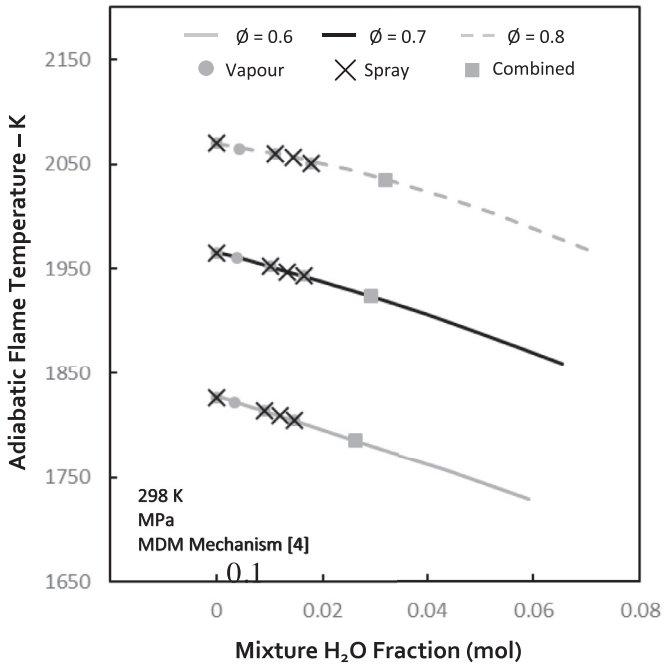

Fig. 3. Change in predicted adiabatic flame temperature against mixture H_2O fraction for the employed converter gas composition at Ø = 0.6, 0.7, and 0.8 with experimental markers.

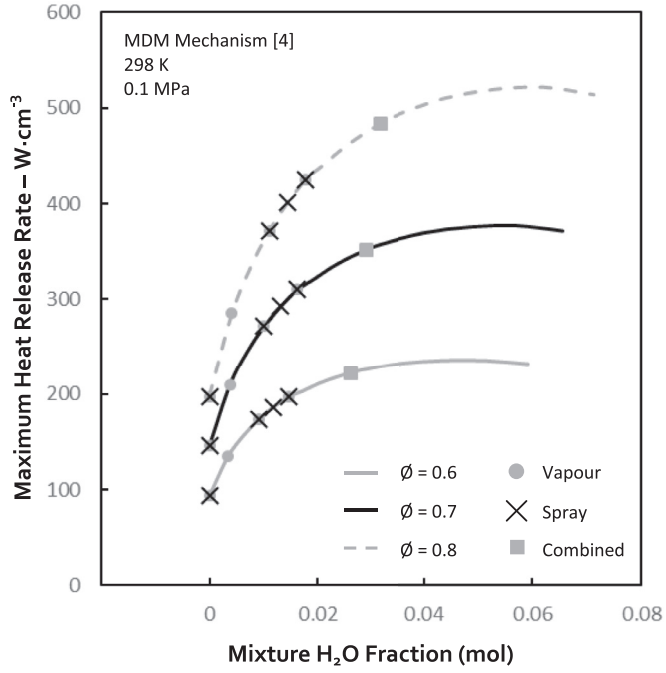

Fig. 4. Change in predicted maximum HRR against mixture H_2O fraction for the employed converter gas composition at Ø = 0.6, 0.7, and 0.8 with experimental markers.

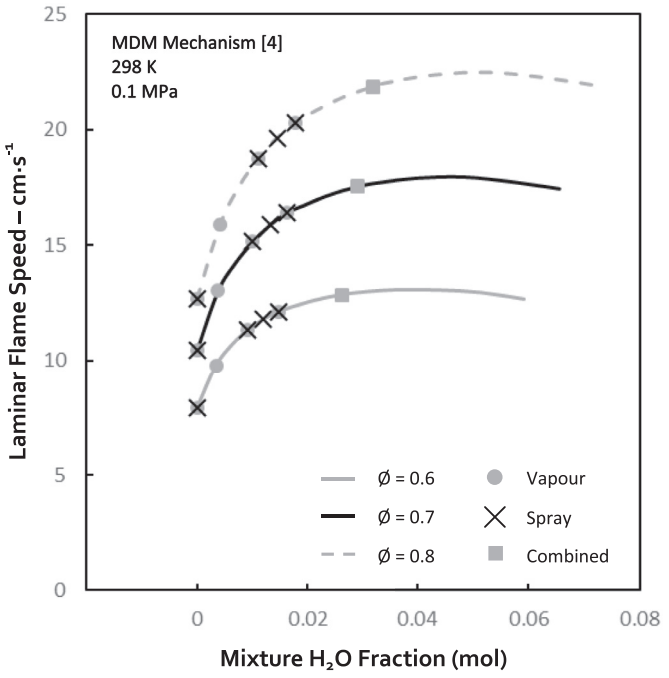

Fig. 5. Change in modelled laminar flame speed against mixture H_2O fraction for the converter gas composition employed at Ø = 0.6, 0.7, and 0.8, with experimental markers.

experimental mass water loadings specified in Section 3 identified as markers for each configuration.

Adiabatic flame temperature is shown to reduce by approximately ~20 K with water loading for each of the three modelled equivalence ratios, and the individual vapour and spray configurations. In comparison, maximum heat release rate significantly increases across the experimental range, more than doubling for the Ø = 0.8 experimental condition, and appearing to peak at H_2O fractions of 0.05–0.06. The overall response is for a faster reaction, as demonstrated with the changes in laminar flame speed presented in Fig. 5 where again, data have been plotted against H_2O fraction, with the experimental data points identified as markers. The increase in flame speed is greater for the richer equivalence ratios; with the highest water loading giving a rise of ~60% for Ø = 0.8, compared to ~53% for Ø = 0.6. This results from the relative difference in molar H_2O fraction of the overall reactant composition, i.e. ~1.8 mol% for Ø = 0.8, compared to ~1.5 mol% for Ø = 0.6. This emphasises the impact that subtle changes in water loading can have with this fuel blend, and suggests that richer mixtures will provide a more significant change in the observed flame response. The increase in flame speed is non-monotonic, peaking at a H_2O fraction of ~0.05. As water loading is increased further, enhancement in HRR diminishes, temperature suppression becomes dominant with a ~75 K reduction in AFT, and the reaction slows [4]. This has been further quantified experimentally using laminar flames with similar mixtures [3,4].

OH was used as a marker for the optical diagnostic techniques employed in the experimental study, and it was therefore important to analyse any potential changes in production that result from H_2O addition. Figure 6 demonstrates the influence of water on the 1-D spatial concentration profiles for two equivalence ratios; Ø = 0.6 and 0.8. Water addition is shown to enhance the production of OH with the given fuel blend through intermediate dissociation, resulting in peak wet concentrations that are almost triple the equivalent dry cases. In addition to catalysing the overall reaction, this increased production of chain carrying radicals also indicated that a broad range of concentrations, or signal intensities was to be expected from the analytical diagnostics.

4.2. Vapour addition to the 100 kW swirl burner

The supply of water vapour was increased at the specified flowrates, with the OH^* chemiluminescence response for Ø = 0.6 shown in Fig. 7- the global signal for projection of half the 3-D flame is shown (a), together with the equivalent Abel inverted image (b), with flow from the bottom up. To improve clarity in

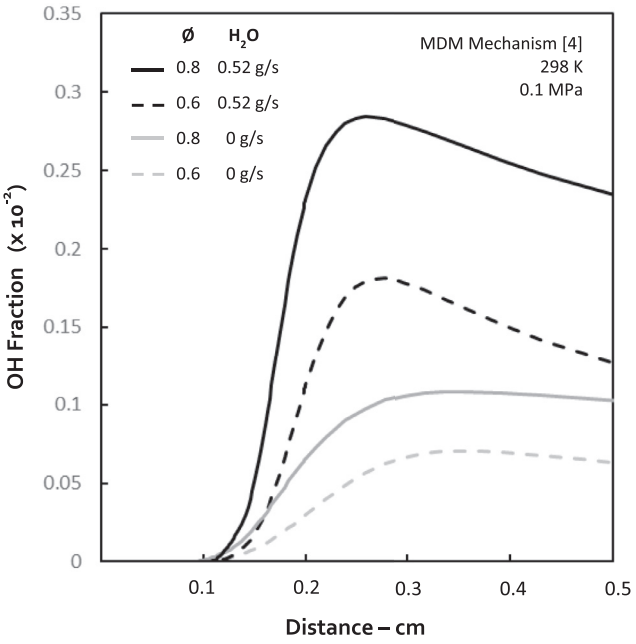

Fig. 6. Modelled 1-D OH spatial concentration profiles for Ø = 0.6 and 0.8, with 0 and 0.52 g s^{-1} H_2O.

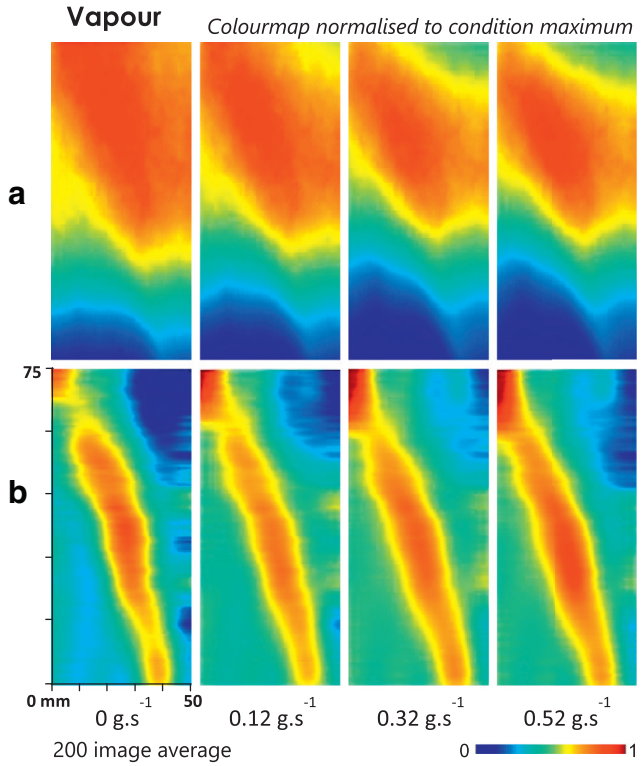

Fig. 7. OH* chemiluminescence signals for projection of the 3-D half flame (a) and equivalent Abel transformed images (b), for Ø = 0.6 with increasing levels of vapour addition.

presentation, intensities are normalised to the maximum intensity in the average image for each condition, with equivalent proportions maintained for all images at the specified scale. The flame was close to the LBO stability limit at the driest condition, with the poorly defined structure appearing elongated. The higher OH* intensities present in the downstream flow are expected, resulting from the overall slower heat release and reaction rates. There also

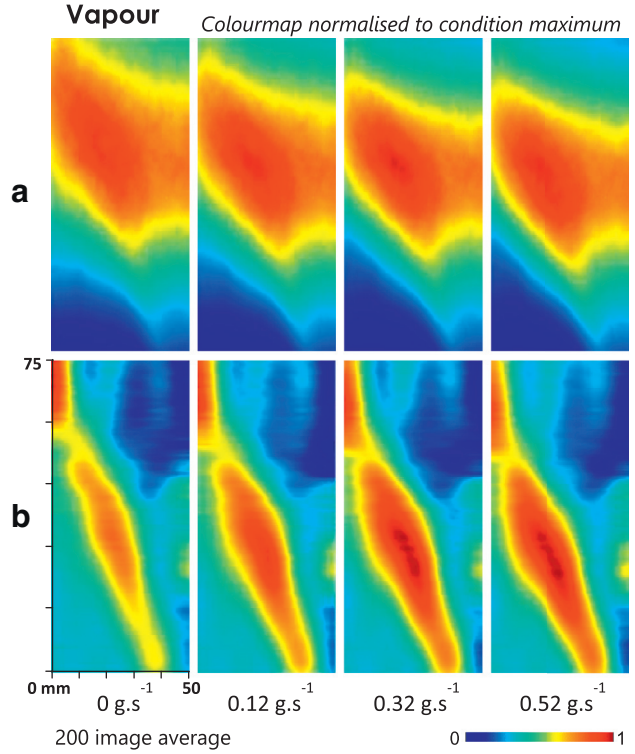

Fig. 8. OH* chemiluminescence signals for projection of the 3-D half flame (a) and equivalent Abel transformed images (b), for Ø = 0.8 with increasing levels of vapour addition.

appears to be higher relative recirculation outside the core forward flow. As the vapour fraction increases, chemical timescales reduce and the flame compresses into a more defined conical structure, with outward flow strengthening and the tip of the inner CRZ becoming more prominent. Chemical kinetics suggest that relative heat release increases with reaction rate – evident outside the shear layer of the premixed swirling flow with marginal thickening of this region observed in the Abel transformed images.

The equivalent images are shown for Ø = 0.8 in Fig. 8, again with a comparison made between the temporally averaged 3-D flame (a), and equivalent Abel transform (b). Compared to the Ø = 0.6 case, heat release in the richer flame does not appear to compact in the same way with the structure already well-defined, but instead transitions further upstream as reaction rate increases. Planar OH profiles were also obtained using the PLIF system with the 25 mm-wide laser sheet, fixed at an axial position 13 mm downstream of the premixed nozzle. These are shown for Ø = 0.6, and 0.8 at each averaged vapour condition in Fig. 9 (note – instantaneous images were processed in the same way, but were shown to endorse the explanation derived from the averaged set and hence are not included). The images show the measured planar OH fluorescence in a horizontal plane positioned at the burner centreline. The unburned reactants from the outward flow are identified by the regions of low signal intensity, with OH measured in the inner and outer recirculation zones. Higher OH concentrations are ostensibly recirculated outside of the forward flow for the driest conditions, with a more uniform intensity distribution across the CRZ. As water vapour concentration increases, signal intensities increase upstream closer to the burner exit, as expected from the increase in reactivity and OH* chemiluminescence results. However, there is also a change in the location of peak relative OH concentration; inasmuch that as vapour flow rises, higher intensities are located inside the shear layer of the CRZ. The 1-D spatial concentration profiles (Fig. 6) suggest a

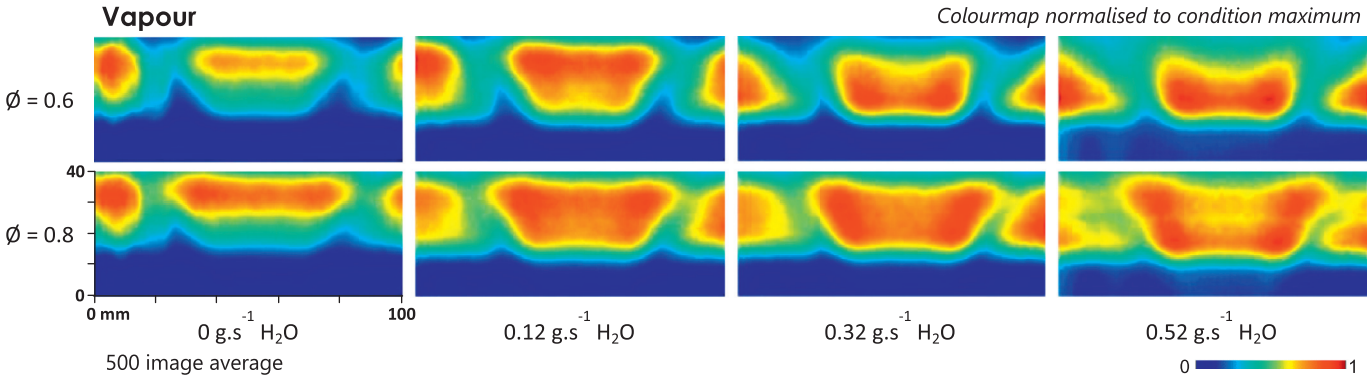

Fig. 9. OH PLIF intensities for Ø = 0.6 and 0.8 with increasing levels of water vapour addition.

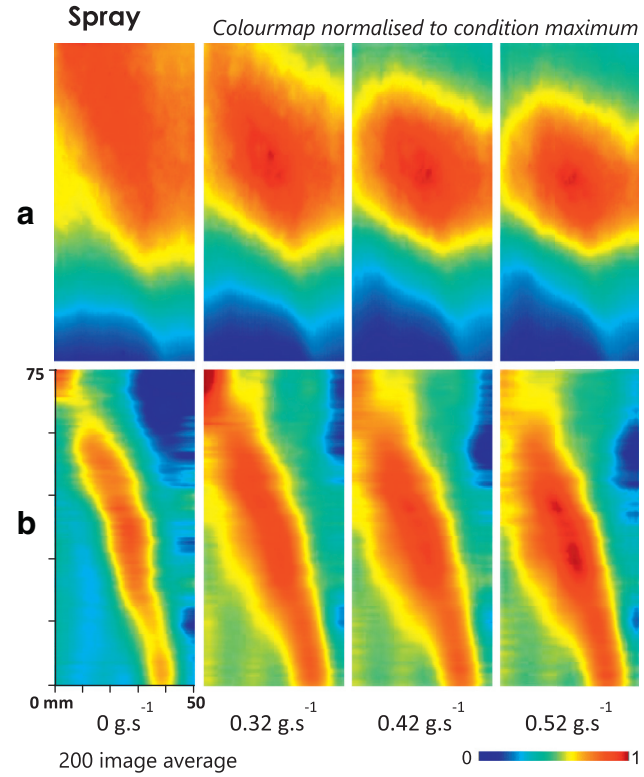

Fig. 10. OH* chemiluminescence signals for projection of the 3-D half flame (a) and equivalent Abel transformed images (b), for Ø= 0.6 with increasing levels of water spray.

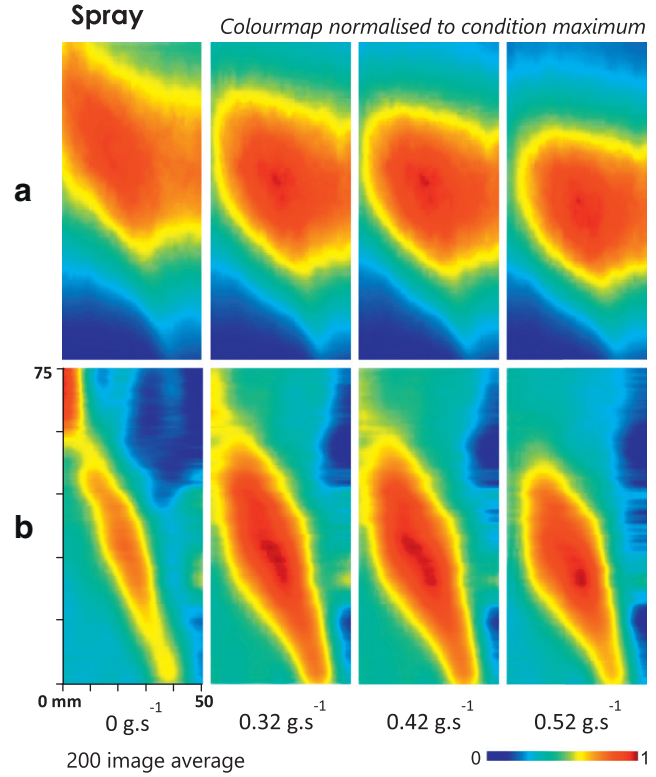

Fig. 11. OH* chemiluminescence signals for projection of the 3-D half flame (a) and equivalent Abel transformed images (b), for Ø = 0.8 with increasing levels of vapour spray.

sharp increase in OH for the wettest conditions followed by a fall, compared to the drier cases where the OH signal reaches a relative plateau. It therefore follows that higher relative concentrations are found closer to the reacting flow, near the axial shear layer boundary and outer recirculation zones.

4.3. Liquid spray addition to the 100 kW swirl burner

The spray angle of the liquid nozzle (60°) was chosen to deliver offset flow into the CRZ, recirculated into the forward flow of reactants. OH* chemiluminescence data were captured for each flow condition, shown with corresponding Abel deconvolution for Ø = 0.6 in Fig. 10. Again, the images show half the symmetrical flame, and have been resized for presentation (fixed proportions are maintained for all images presented, equivalent to those shown in Figs. 7 and 8). As the droplets are delivered into the CRZ, the flame experiences enhancement due to the effects of catalytic chemical dissociation, contrasted against heat loss and a change in local strain and turbulence intensity resulting from spray dynamics and droplet transportation [33]. The net effect is to compact and narrow the flame structure, shortening the area of localised heat release by a greater amount than the equivalent vapour experiments.

Similar influences are evident for the Ø = 0.8 case shown in Fig. 11, as the flame retracts upstream and spray flowrate increases. Again, overall flame size reduces compared with the equivalent vapour cases shown in Fig. 8. The Abel inverted images suggest a shortening of the flame structure, as peak heat release intensities move from the boundary confinement, chemical timescales are reduced locally and the CRZ contracts, trends that are also evident in the OH PLIF results: Fig. 12(a) gives a comparison between the average Ø = 0.8 spray and vapour experiments with the laser plane fixed in an equivalent position; ~13 mm downstream of the

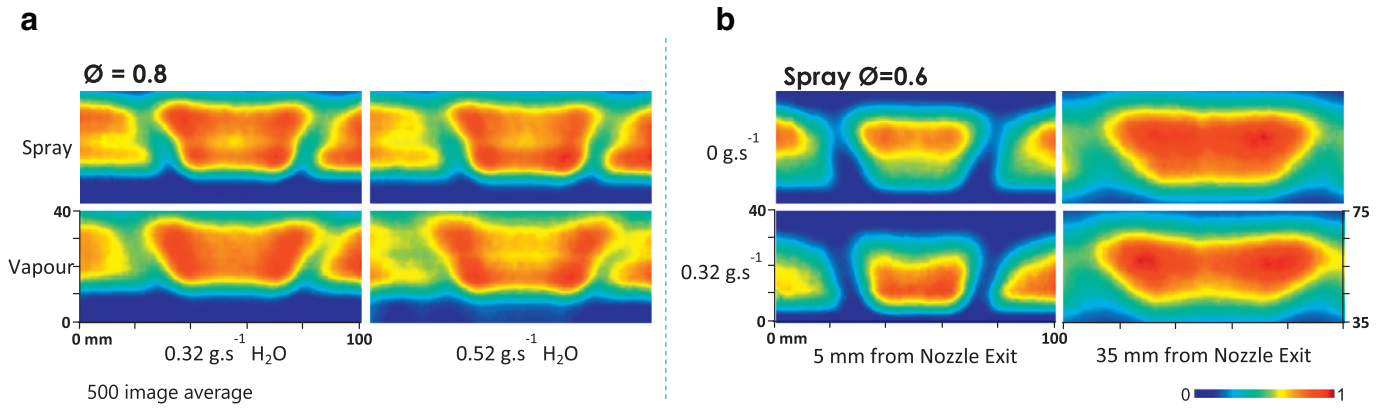

Fig. 12. (a) Comparison between centreline OH PLIF planes positioned 13 mm downstream from the burner nozzle, for equivalent vapour and spray experiments at Ø = 0.8. (b) Influence of water spray addition on centreline OH PLIF planes at different downstream axial locations at Ø = 0.6, note the difference in y-axis scales.

burner exit nozzle. OH fluorescence from the spray experiments indicate a marginal narrowing of the CRZ with an overall width reduction of 12–16% (calculated from the geometry of the scaled mages), and larger areas of recirculated OH present outside the forward flow. In addition, higher OH intensities are observed again on the outer boundary of the CRZ, near the axial shear layer. This is present in greater detail in Fig. 12(b), where data have been collected at different axial locations in the Ø = 0.6 flame.

The 25 mm-wide laser sheet was repositioned at downstream distances of 5 mm and 35 mm, on the centreline from the burner exit nozzle. Further data was collected for the driest experiments, with the introduction of the spray again causing a relative increase in the average measured upstream OH intensities, as reaction rate increases and the flame changes position. This is also apparent in the data collected 35 mm downstream, with the retracted flame wider for the wetter test. The dry case appears to have a more consistent OH intensity distribution across the tangential flame profile, with peaks forming in the outer layer of the CRZ at the 0.32 g s^{-1} condition. Again, this is likely to result from peaks in OH production profiles observed in Fig. 6, relative to the localised outward reacting flow. Introduction of the spray is expected to cause some inhomogeneity in the reaction zone as H_2O is entrained into the recirculated flow, and may also result in localised OH production.

In addition to inhomogeneity and change in phase, there are other subtle differences between the two experimental configurations which influence the flame. The increase in bulk exit velocities (1.8% worst-case) and flow dynamics resulting from the introduction of vapour apply to the entire outward flow field. Whereas the premixed gaseous exit velocities remain constant for the spray experiments, with the additional flow, and change in turbulence intensity, introduced locally to the CRZ from water dispersion and transportation. In addition, the introduction of a liquid spray further reduces flame temperature by an additional ~20 K for the highest flowrates, resulting from the latent heat required for phase change. This is shown in Fig. 13, where comparisons of the measured combustor exhaust temperature (T3) have been plotted – averaged for all equivalence ratios for simplicity in presentation – against experimental water mass loading. Burner face temperatures (T2) measured during the vapour experiments have also been included. An expected temperature rise is noted as vapour concentration increases, and the flame retracts upstream toward the outlet nozzle and burner face. This demonstrates the significant (200–300 K) fluctuation in operational temperatures that may be experienced with the utilisation of this fuel blend from subtle changes in atmospheric humidity. The combined effect of this change in temperature with reaction rate also creates the potential for further change in flame topology or premixed

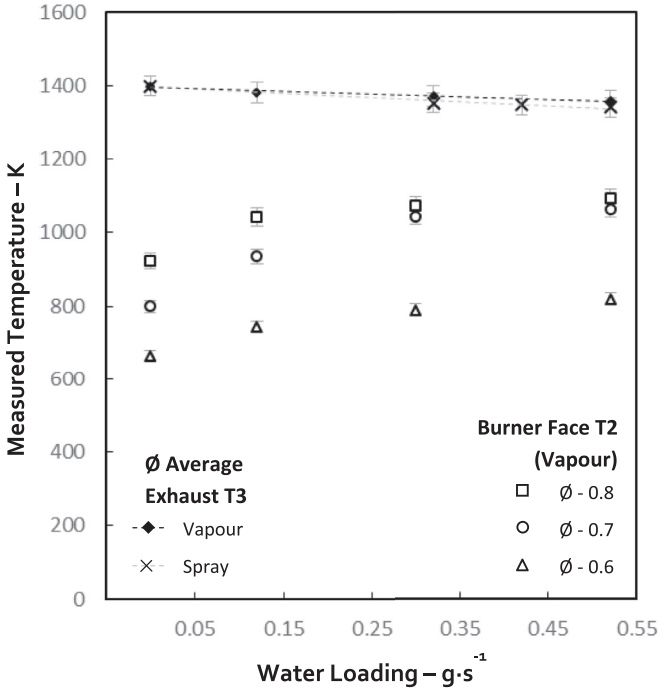

Fig. 13. Change in measured exhaust (T3) and burner face temperatures (T2) resulting from water addition.

flashback, which could possibly occur with a different burner configuration, or a change in outlet velocities [34,35].

4.4. Two-phase vapour spray addition

The combined influence of two-phase vapour spray flow was investigated to further analyse the mechanisms through which the flame structure may be influenced by water addition, so enhancing premixed operational stability. Figure 14 shows a comparison between the OH* chemiluminescence intensities obtained at Ø = 0.7 with equivalent flow conditions for the vapour and spray experiments, in addition to both combined at the highest vapour flow rate. Again, the global signal for projection of half the 3-D flame is shown (a) together with equivalent Abel deconvolution (b), and image proportions maintained from results presented previously.

The heat release trends evident for each of the distinct vapour and spray experiments correspond to those presented earlier, with the overall structure compacting and the flame retracting

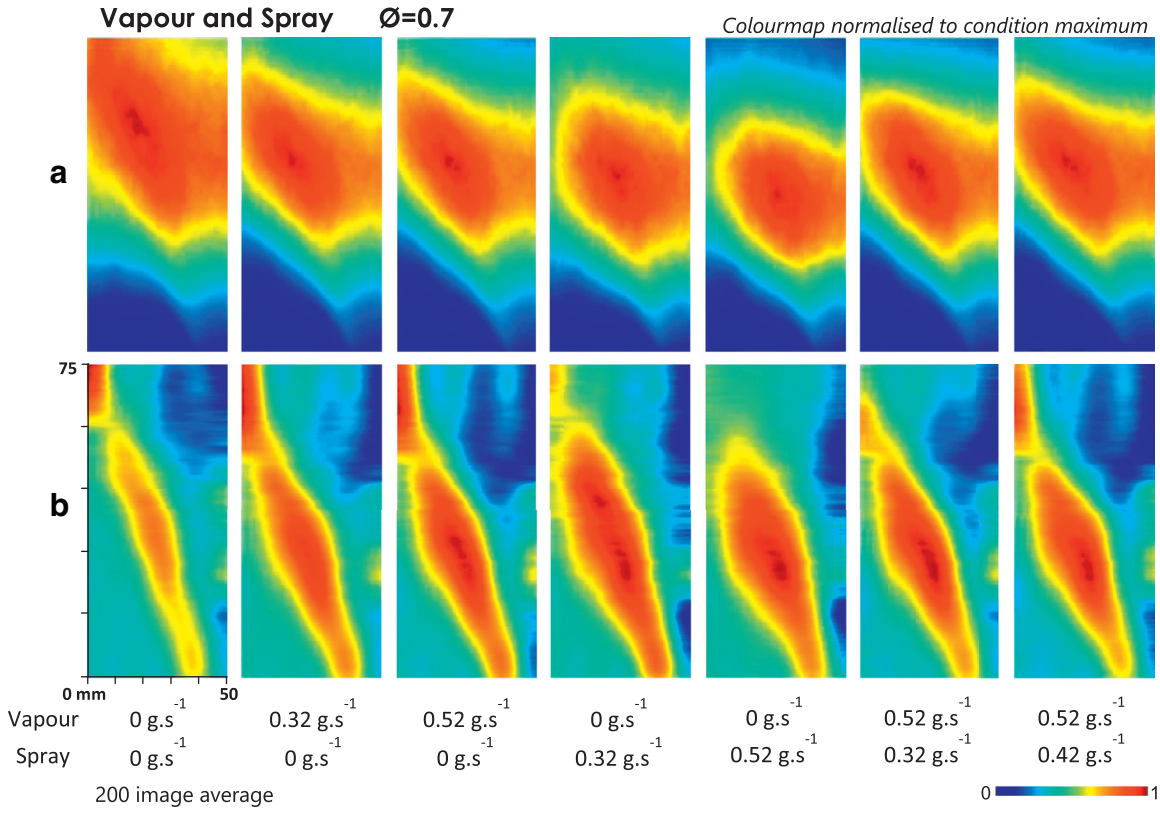

Fig. 14. OH* chemiluminescence signals for projection of the 3-D half flame (a) and equivalent Abel transformed images (b), for Ø = 0.7 with increasing levels of two-phase water addition.

upstream in the flow. Spray addition is again shown to produce narrowing of the heat release profile, drawing in the CRZ and shortening the flame. Operation was shown to be stable at all conditions of two-phase flow considered, with a significant characteristic observed; initially introduction of the spray causes the heat release structure to compact from the equivalent 0.52 g s^{-1} vapour only case. This may be expected given the changes observed from the spray experiments. However, as liquid flow is increased the flame structure is shown to expand and elongate, giving closer resemblance to the vapour only results. This tendency was also observed for the Ø = 0.6 and 0.8 experiments, and suggests that the narrowing of the shortened flame results more from the local catalytic influence of H_2O introduction to the CRZ, than the turbulence induced from droplet introduction in the spray. The chemical enhancement resulting from dissociation has peaked at the highest flow conditions, and is in competition with the thermal effect of water acting more as a traditional diluent, increasing chemical timescales and slowing the reaction [4], as quantified in Figs. 3–6 Section 4.1. Therefore at higher flow conditions the local influence of H_2O on the CRZ is lessened, and the heat release structure reverts back to the vapour form. An equivalent peak was observed in the burner face temperature (T2), with values falling as the combined flow began to elongate the flame.

The catalytic enhancement in flame speed also provided an extension of the LBO stability limit, with detachment of the flame from the anchor. As the chemical structure compacted and overall reaction rate increased, air flows could be driven higher to give leaner equivalence ratios. Using the methodology outlined in Section 3, the LBO stability limit was determined for each configuration and flow condition with the corresponding equivalence ratios plotted in Fig. 15, where error bars represent the combined uncertainty in flow metering and fuel delivery

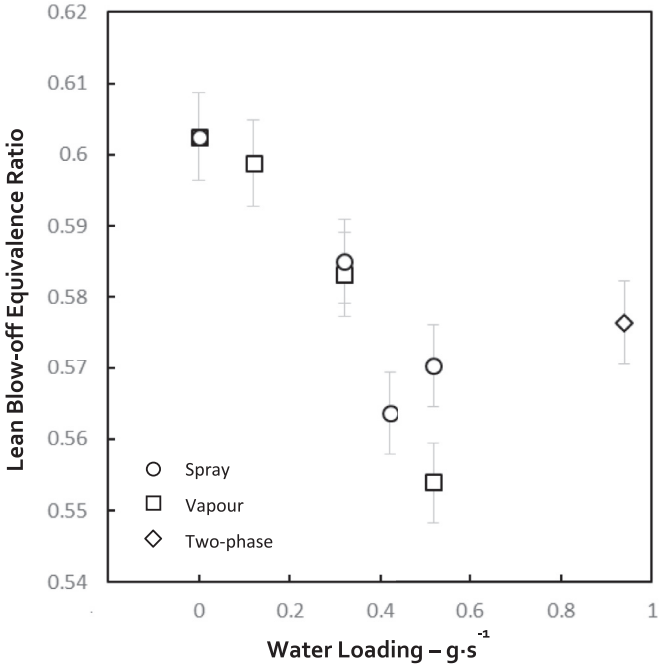

Fig. 15. Change in LBO equivalence ratio for all experimental configurations.

Water addition is shown to expand the lean stability envelope of the given fuel blend. Stable air flows increase by almost 10% for the addition of 0.52 g s^{-1} water, with vapour delivery providing leaner limits compared to the equivalent spray conditions. This

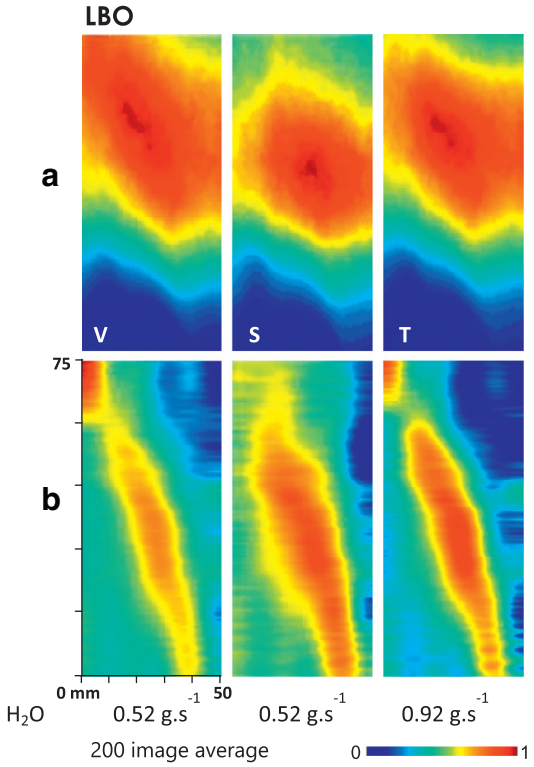

Fig. 16. OH* chemiluminescence signals for projection of the 3-D half flame (a) and equivalent Abel transformed images (b) for LBO conditions (V-vapour, S-spray, T-two-phase).

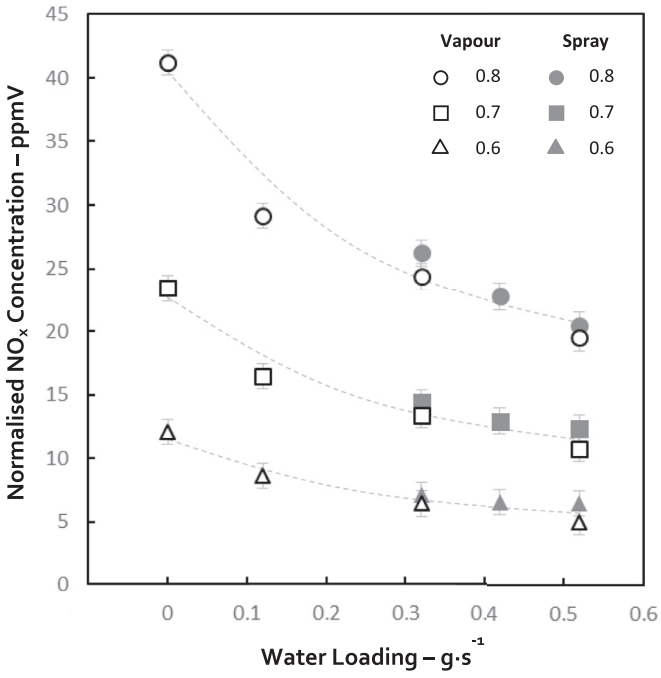

Fig. 17. Change in normalised (dry,15% O_2) NO_x concentration with water loading for Ø = 0.6–0.8.

is attributed to the additional heat loss experienced from the phase change necessary with the liquid supply, and potential inhomogeneity in the reaction zone. The two-phase water case demonstrates a shift in the trend, with an increase in the lean stability limit equivalence ratio. Kinetic results demonstrated the catalytic enhancement saturating at these flowrates, with flame temperature and heat release rate reduced, and chemical timescales extended. It could therefore be projected that a further increase in water supply would limit the stability envelope further, eventually reducing it below the driest case. A permanent water spray therefore has the potential to reduce some of the operational fluctuations that may result from change in atmospheric humidity, but flow rates have to be carefully specified. OH* chemiluminescence was employed to characterise heat release distribution at the wettest conditions at the stable lean limit, with results shown in Fig. 16. There is an increase in heat release recirculated outside of the forward flow for all conditions, as the flame extends into the outer recirculation zones. The vapour and two-phase experiments show the flame elongated, and the structure more apparent than the dry Ø = 0.6 case (Figs. 7 and 10). However, the local catalytic influence of H_2O in the CRZ gives the spray condition the narrow structure previously observed, and the corresponding Abel deconvolution shows a larger zone of heat release. Detachment of the spray flame can therefore be attributed to localised heat loss near the anchor at burner outlet, as opposed to a reduction of global chemical reactivity seen with the vapour case, and hence why the stability limit is comparatively reduced.

4.5. Emission measurements

Emission measurements were made using the analytical setup outlined in Section 2.4. Total NO_x concentrations were measured hot and wet, and data were therefore normalised in accordance with BS EN 11,042 [28] prior to presentation: First the measurement (θ_{meas}) was normalised to an equivalent dry reading (θ_{dry}) using the corresponding exhausted water fraction (X_{H_2O}) for each experimental condition, obtained from the chemical models detailed in Section 3, shown in Eq. (1).

$$\theta_{dry} = \theta_{meas} \cdot \left(\frac{1}{1 - X_{H2O}}\right) \quad (1)$$

The dry component was then normalised equivalent to 15% O_2 ($\theta_{dry,15\%O2}$) dilution using the measured O_2 concentrations (θ_{O2}), presented in Eq. (2).

$$\theta_{dry,15\%O2} = \theta_{dry} \cdot \left(\frac{20.9 - 15}{20.9 - \theta_{O2}}\right) \quad (2)$$

CO was analysed dry and therefore only required normalising to the equivalent 15% O_2 condition. Normalised total NO_x concentrations were obtained for the vapour and spray experimental configurations, and are shown for Ø = 0.6–0.8 in Fig. 17 trend lines have been superimposed for clarity. The error bars represent total uncertainty in the measurement system, and comprise analyser specifications, linearisation, and accuracy in span gas certification. H_2O introduction is shown to approximately halve the normalised NO_x concentrations for each equivalence ratio across the 0–0.52 g s^{-1} range. This reduction results from a drop thermal NO_x production with adiabatic flame temperature [8,13–15], and also provides the offset between each equivalence ratio. Work undertaken by Zhao et al. [13] demonstrated that H_2O can lead to a kinetic increase in NO_x production from the rise in OH concentration at constant temperature, however this effect is eclipsed by thermal influences and HCN formation. It is noteworthy that for the spray experiments, NO_x concentrations are consistently higher than the equivalent vapour case. Even with lower global temperatures resulting from H_2O phase change, the spray experiments feed locally into the CRZ and therefore potentially allow for the formation of localised hotter, drier combustion regions. Similar results were obtained by Furuhata et al. [36] with variation in NO_x concentrations resulting from changes in steam injection location, and localised hotter regions in the flame.

With water addition shown to facilitate leaner operation (Section 4.3), the potential for further NO_x reduction was

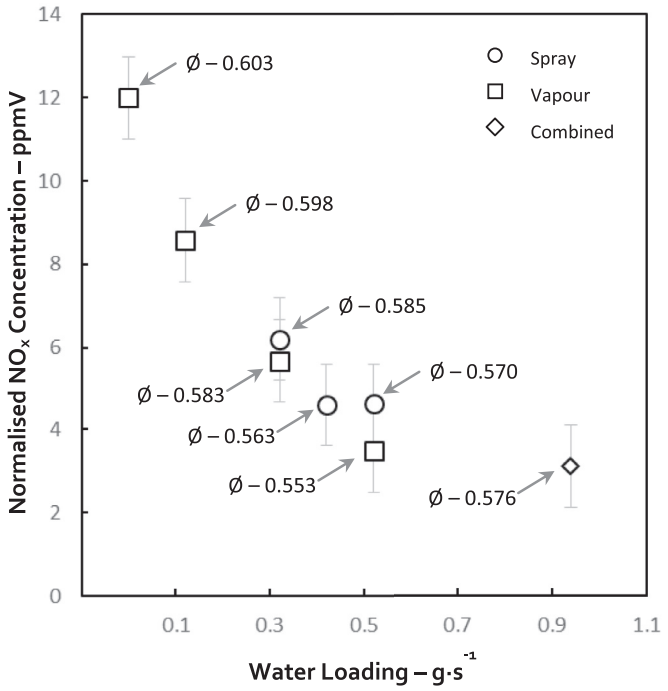

Fig. 18. Change in normalised (dry,15% O_2) NO_x concentration with water loading at the lean stability limit.

quantified for the leanest stable equivalence ratio at each flow condition. The results are shown plotted against change in water loading in Fig. 18. From initial dry concentrations of ~12 ppmV at Ø = 0.6, further normalised reduction by a factor of four is recorded for the highest experimental water addition. Again, vapour cases provided marginally lower values as a result of the inhomogeneous spray mix. CO concentrations were also quantified and demonstrated an equivalent trend of reduction with an increase in water loading and lowering of equivalence ratio, dropping from a peak value of ~18 ppmV at Ø = 0.8 to ~5 ppmV for the wettest and leanest conditions. This shift in production is again attributed to change in flame temperature and the employed premixed burner configuration [15,37].

5. Conclusions

As predicted from a recent laminar flame study, subtle changes in H_2O fraction had a substantial, counter-intuitive, impact on the premixed combustion behaviour of a converter gas in a premixed turbulent, swirling flame. In addition to reducing flame temperature, H_2O dissociation enhances chain carrier formation, catalysing CO oxidation and increasing reactivity and heat release rate. Changes in vapour H_2O concentration to levels representative of fluctuation in atmospheric humidity – up to 1.8% mol – were shown to enhance laminar flame speed by up to 60%. The impact of this change on a premixed swirling flame is dependent on equivalence ratio; near the lean stability limit, an increase compresses the area of localised heat release to shorten the elongated flame structure. However with a stable and well-defined flame structure, vapour addition triggers a change in axial heat release location, causing the flame front to retract upstream toward the burner outlet nozzle.

An atomised spray was employed to deliver equivalent quantities of liquid H_2O into the CRZ of the premixed flame. Local catalytic H_2O dissociation and turbulence resulting from droplet evaporation combine to provide qualitatively similar but more significant change in heat release. The flame structure is again compressed, moving upstream toward the premixed nozzle outlet with an increase in H_2O flowrate. However, compared to vapour addition, the spray provides localised narrowing in the heat release structure. This results from the local influence of H_2O in the CRZ, with the flame reverting back to the vapour structure as water concentrations are further increased with two-phase flow, and the catalytic influence of chain carrying species formation is diminished. The spray also causes detachment at the lean stability limit through localised heat loss, compared to the vapour case.

Practical operability of the employed burner configuration was sensitive to subtle changes in H_2O loading with either a vapour or liquid spray: Altering overall reactant composition by 1.8% mol gave rise to changes in measured surface temperatures of up to ~300 K as a function of equivalence ratio. H_2O induced increase in overall reaction rate also caused a change in the lean stability limit; excess air could be increased by almost 10% with the employed configuration at the highest experimental vapour loading. The observed changes in flame response also highlight the potential for changes in flame topology or other premixed instabilities such as flashback. The permanent addition of a water spray could dampen fluctuations due to changes in atmospheric humidity, as the flame was stable with two-phase H_2O flow. However, the delivery rate must be carefully specified as the catalytic influence of H_2O is diminished with excessive supply, and the reaction quenched.

There is potential for the significant reduction of NO_x and CO emissions from using water as a stability mechanism with the employed flame. NO_x concentrations approximately halved for each experimental equivalence ratio with loading in either the vapour or liquid phase. This was further reduced with the reduction in LBO equivalence ratio, lowering flame temperature. Concentrations dropped to a third of the equivalent dry value for 0.52 g s^{-1} supply, and were reduced further by a factor of four with the addition of both vapour and spray at the highest flow conditions.

Acknowledgments

The inspiration for this work was provided by an ongoing industrial partnership with TATA Steel/EU, and supported by funding from the UK's Engineering and Physical Sciences Research Council project reference EP/M015300/1. Information on the data underpinning the results presented here, including how to access them, can found at Cardiff University data catalogue at http://doi.org/10.17035/d.2016.0011507413. The research was undertaken at the Cardiff University's Gas Turbine Research Centre (GTRC) with invaluable technical support from Jack Thomas and Terry Treherne.

References

[1] R. Remus, M.A. Aguado-Monsonet, S. Roudier, L.D. San, Best available techniques reference document on the production of iron and steel, IPPC European Commission, 2013 Industrial Emissions Directive 2010/75/EU.
[2] D.G. Pugh, Combustion characterisation of compositionally dynamic steelworks gases Ph.D. Thesis, Cardiff University, U.K., 2014.
[3] A.K. Das, K. Kumar, C. Sung, Laminar flame speeds of moist syngas mixtures, Combust. Flame 158 (2011) 345–353.
[4] D.G. Pugh, A.P. Crayford, P.J. Bowen, M. Al-Naama, Parametric investigation of water loading on heavily carbonaceous syngases, Combust. Flame 164 (2016) 126–136.
[5] Y. Xie, J. Wang, N. Xu, S. Yu, M. Zhang, Z. Huang, Thermal and chemical effects of water addition on laminar burning velocity of syngas, Energy Fuel. 28 (2014) 3391–3398.
[6] D.G. Pugh, A.P. Crayford, P.J. Bowen, T. O'Doherty, R. Marsh, Variation in laminar burning velocity and Markstein length with water addition for industrially produced syngases, ASME Turbo Expo 2014 (2014) Paper GT2014-25455.
[7] D. Singh, T. Nishiie, S. Tanvir, L. Qiao, An experimental and kinetic study of syngas/air combustion at elevated temperatures and the effect of water addition, Fuel 94 (2012) 448–456.
[8] B. Ge, Y. Tian, S. Zang, The effects of humidity on combustion characteristics of a nonpremixed syngas flame, Int. J. Hydrogen Energy 41 (2016) 9219–9226.
[9] J. Santner, F. Dryer, Y. Ju, Effect of water content on syngas combustion at elevated pressure, 50th AIAA Aerospace Sciences Meeting (2012) Paper AIAA 2012-0163.

[10] A. Bagdanavicius, P.J. Bowen, D. Bradley, M. Lawes, M.S. Mansour, Stretch rate effects and flame surface densities in premixed turbulent combustion up to 1.25 MPa, Combust. Flame 162 (2015) 4158–4166.
[11] S.A. Filatyev, J.F. Driscoll, C.D. Carter, J.M. Donbar, Measured properties of turbulent premixed flames for model assessment, including burning velocities, stretch rates, and surface densities, Combust. Flame 141 (2005) 1–21.
[12] C.K Law, Combustion physics, Cambridge University Press, U.K., 2006.
[13] D. Zhao, H. Yamashita, K. Kitagawa, N. Arai, T. Furuhata, Behavior and effect on NO_x formation of OH radical in methane–air diffusion flame with steam addition, Combust. Flame 130 (2002) 352–360.
[14] G.J. Rørtveit, J.E. Hustad, S. Li, F.A. Williams, Effects of diluents on NO_x formation in hydrogen counterflow flames, Combust. Flame 130 (2002) 48–61.
[15] S. Göke, M. Füri, G. Bourque, B. Bobusch, K. Göckeler, O. Krüger, S. Schimek, S. Terhaar, C.O. Paschereit, Influence of steam dilution on the combustion of natural gas and hydrogen in premixed and rich-quench-lean combustors, Fuel Process. Technol. 107 (2013) 14–22.
[16] G. Cabot, D. Vauchelles, B. Taupin, A. Boukhalfa, Experimental study of lean premixed turbulent combustion in a scale gas turbine chamber, Exp. Therm. Fluid Sci. 28 (2004) 683–690.
[17] C.S. Panoutsos, Y. Hardalupas, A.M.K.P. Taylor, Numerical evaluation of equivalence ratio measurement using $OH*$ and $CH*$ chemiluminescence in premixed and non-premixed methane–air flames, Combust. Flame 156 (2009) 273–291.
[18] M. Lauer, T. Sattelmayer, Heat release calculation in a turbulent swirl flame from laser and chemiluminescence measurements, 14th International Symposium on Applications of Laser Techniques to Fluid Mechanics (2008).
[19] N.A. Chigier, J.M. Beer, The flow region near the nozzle in double concentric jets, J. Basic Eng. 4 (1964) 797–804.
[20] H.J. Sheen, W.J. Chen, S.Y. Jeng, T.L. Huang, Correlation of swirl number for a radial-type swirl generator, Exp. Therm. Fluid Sci. 12 (1996) 444–451.
[21] R. Marsh, J. Runyon, A. Giles, S. Morris, D.G. Pugh, A. Valera-Medina, P.J. Bowen, Premixed methane oxycombustion in nitrogen and carbon dioxide atmospheres: measurement of operating limits, flame location and emissions, Proc. Combust. Inst. (2016), doi:10.1016/j.proci.2016.06.057.
[22] S. Taamallah, S.J. Shanbhogue, A.F. Ghoniem, Turbulent flame stabilization modes in premixed swirl combustion: physical mechanism and Karlovitz number-based criterion, Combust. Flame 166 (2016) 19–33.
[23] C. Killer, Abel Inversion Algorithm, http://www.mathworks.com/matlabcentral/fileexchange/43639-abel-inversion-algorithm, 2013 (accessed 01/12/2015).
[24] S.J. Shanbhogue, Y.S. Sanusi, S. Taamallah, M.A. Habib, E.M.A. Mokheimer, A.F. Ghoniem, Flame macrostructures, combustion instability and extinction strain scaling in swirl-stabilized premixed CH_4/H_2 combustion, Combust. Flame 163 (2016) 494–507.
[25] J. Runyon, R. Marsh, Y. Sevcenco, D. Pugh, S. Morris, Development and commissioning of a chemiluminescence imaging system for an optically-accessible high-pressure generic swirl burner, 7th European Combustion Meeting (2015) Paper P3-29.
[26] S. Krishna, R. Ravikrishna, Quantitative OH planar laser induced fluorescence diagnostics of syngas and methane combustion in a cavity combustor, Combust. Sci. Technol. 187 (2015) 1661–1682.
[27] U. Stopper, W. Meier, R. Sadanandan, M. Stöhr, G.Bulat M.Aigner, Experimental study of industrial gas turbine flames including quantification of pressure influence on flow field, fuel/air premixing and flame shape, Combust. Flame 160 (2013) 2103–2118.
[28] British Standard ISO 11042-1:1996, Gas turbines. Exhaust gas emission, Measurement and evaluation, British Standards Institution, U.K., 1996.
[29] Delevan Nozzle Technology Report, http://www.delavan.co.uk/pdfs/ntg.pdf, (accessed 01/07/2015).
[30] R.J. Kee, F.M. Rupley, J.A. Miller, M.E. Coltrin, J.F. Grcar, E. Meeks, H.K. Moffat, A.E. Lutz, G. Dixon-Lewis, M.D. Smooke, J. Warnatz, G.H. Evans, R.S. Larson, R.E. Mitchell, L.R. Petzold, W.C. Reynolds, M. Caracotsios, W.E. Stewart, P. Glarborg, C. Wang, O. Adigun, CHEMKIN collection release 3.6, Reaction Design, San Deigo, USA, 2000.
[31] CHEMKIN-PRO 15131, Reaction design: San Diego, 2009. http://www.reactiondesign.com/support/help/help_usage_and_support/how-to-cite-products/.
[32] S.G. Davis, A.V. Joshi, H. Wang, F. Egolfopoulos, An optimized kinetic model of H_2/CO combustion, Proc. Combust. Inst. 30 (2005) 1283–1292.
[33] J. Xia, H. Zhao, A. Megaritis, K.H. Luo, A. Cairns, L.C. Ganippa, Inert-droplet and combustion effects on turbulence in a diluted diffusion flame, Combust. Flame 160 (2013) 366–383.
[34] T.F. Guiberti, D. Durox, L. Zimmer, T. Schuller, Analysis of topology transitions of swirl flames interacting with the combustor side wall, Combust. Flame 162 (2015) 4342–4357.
[35] P. Sayad, A. Schönborn, J. Klingmann, Experimental investigation of the stability limits of premixed syngas-air flames at two moderate swirl numbers, Combust. Flame 164 (2016) 270–282.
[36] T. Furuhata, T. Kawata, N. Mizukoshi, M. Arai, Effect of steam addition pathways on NO reduction characteristics in a can-type spray combustor, Fuel 89 (2010) 3119–3126.
[37] H. Kobayashi, S. Yata, Y. Ichikawa, Y. Ogami, Dilution effects of superheated water vapor on turbulent premixed flames at high pressure and high temperature, Proc. Combust. Inst. 32 (2009) 2607–2614.